Journal of Hydrology X 9 (2020) 100063

Contents lists available at ScienceDirect

Journal of Hydrology X

journal homepage: www.journals.elsevier.com/journal-of-hydrology-x

Research papers

A synthetic experiment to investigate the potential of assimilating LAI through direct insertion in a land surface model

Azbina Rahman[a,*], Xinxuan Zhang[a], Yuan Xue[a], Paul Houser[a], Timothy Sauer[a], Sujay Kumar[b], David Mocko[b], Viviana Maggioni[a]

[a] George Mason University, Fairfax, VA 22030, United States
[b] National Aeronautics and Space Administration (NASA), Greenbelt, MD 22071, United States

ARTICLE INFO

Keywords:
Data assimilation
Direct insertion
Leaf area index
Dynamic vegetation model (DVM)
Land surface model (LSM)
Land information systems (LIS)

ABSTRACT

This study evaluates the potential of assimilating phenology observations using a direct insertion (DI) method by constraining the modeled terrestrial carbon dynamics with synthetic observations of vegetation condition. Specifically, observations of leaf area index (LAI) are assimilated in the Noah-Multi Parameterization (Noah-MP) land surface model across the continental United States during a 5-year period. An observing system simulation experiment (OSSE) was developed to understand and quantify the model response to assimilating LAI information through DI when the input precipitation is strongly biased. This is particularly significant in data poor regions, like Africa and South Asia, where satellite and re-analysis products, known to be affected by significant biases, are the only available precipitation data to drive a land surface model. Results show a degradation in surface and rootzone soil moisture after assimilating LAI within Noah-MP, but an improvement in intercepted liquid water and evapotranspiration with respect to the open-loop simulation (a free run with no LAI assimilation). In terms of carbon and energy variables, net ecosystem exchange, amount of carbon in shallow soil, and surface soil temperature are improved by the LAI DI, although canopy sensible heat is degraded. Overall, the assimilation of LAI has larger impact in terms of reduced systematic and random errors over the Great Plains (cropland, shrubland, and grassland). Moreover, LAI DA shows a greater improvement when the input precipitation is affected by a positive (wet) bias than the opposite case, in which precipitation shows a dry bias.

1. Introduction

Vegetation supports critical functions in the biosphere as it regulates both the biogeochemical (water, carbon, and nitrogen) and energy cycles from the local to the global scale. Vegetation also strongly affects soil characteristics, including soil volume, chemistry, and texture, which has a feedback on various vegetation characteristics, including productivity and structure (Kumi-Boateng et al., 2012). Vegetation dynamics are therefore crucial when modeling the land surface (Littell et al., 2011). Dynamic vegetation models (DVMs) have been designed to represent structural and functional variables that control land-surface energy, carbon, nutrient, and water budgets (Wullschleger et al., 2014, Peterson et al., 2014). DVMs and land surface models (LSMs) have been combined in the past to improve the estimation of water, carbon, and energy cycle processes (Clark et al., 2011, Dai et al., 2003). For instance, the Noah Multi-Parameterization LSM (hereinafter Noah MP) developed by Niu et al. (2011) uses multiple options for key land hydrologic processes together with a module that allocates carbon to various parts of vegetation and soil carbon pools.

Satellite observations offer a valid alternative for monitoring vegetation globally, producing maps of indices such the Leaf Area Index (LAI), defined as the one-sided leaf surface area measured over unit ground, and the Normalized Difference Vegetation Index (NDVI), based on spectral reflectance measurements acquired in the red and near-infrared regions. LAI has been proven to be a useful indicator of the exchange of water vapor and CO_2 between the vegetation canopy and atmosphere (Xiao et al., 2016; Albergel et al., 2017), whereas NDVI is an indicator of the density of green vegetation on a patch of land (Yang et al., 2012). For example, the Moderate Resolution Imaging Spectroradiometer (MODIS) has been acquiring data in 36 spectral bands since 2000 (Rees and Danks, 2007) at resolutions of 500–1000 m every 4–8 days, and the Advanced Very High-Resolution Radiometer (AVHRR; Tucker et al., 2005) produces global maps of LAI at a resolution of 4 km every 10 days.

Nevertheless, satellite-based observations often have gaps in their spatial and temporal coverage (mainly due to cloud coverage). In order

* Corresponding author.
E-mail address: arahma19@gmu.edu (A. Rahman).

https://doi.org/10.1016/j.hydroa.2020.100063
Received 11 March 2020; Received in revised form 3 September 2020; Accepted 6 September 2020
Available online 11 September 2020

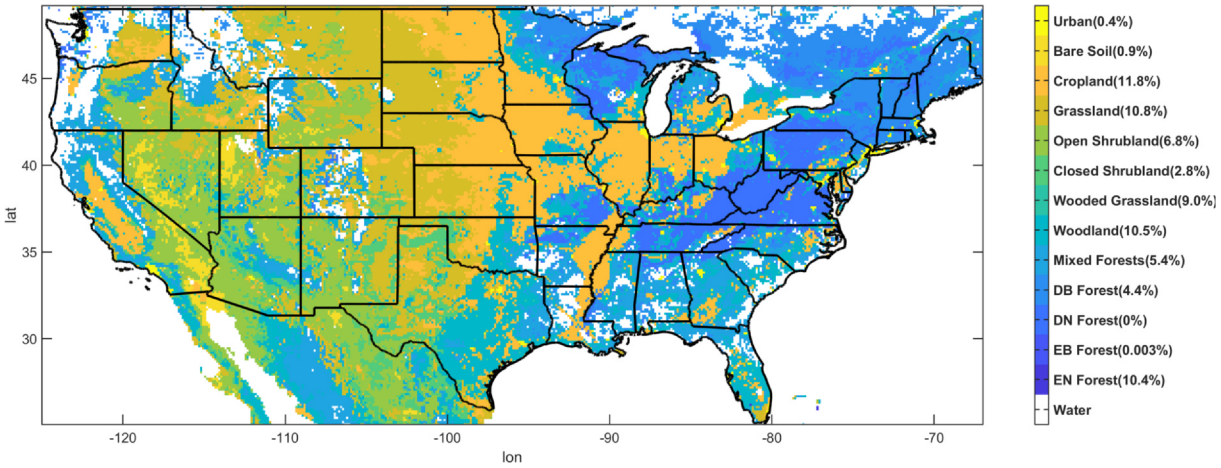

Fig. 1. Land surface classification by MODIS used in the Noah-MP model across the study region. The percentage area for each class is shown in the legend (EN: Evergreen Needleleaf; EB: Evergreen Broadleaf; DN = Deciduous Needleleaf; DB: Deciduous Broadleaf).

to fill in such gaps and guarantee continuous time series, observations are commonly merged with model simulations. Data assimilation is a well-known technique for optimally combining the information from such observations and model estimates based on their respective uncertainties (Reichle, 2008). Land Data Assimilation Systems (LDASs) have been successfully used in the past decades to merge satellite observations of soil moisture and surface temperature into LSMs (e.g., Reichle et al., 2008, Reichle, 2008, Maggioni and Houser, 2017). In the recent past, a few attempts applied the same concept to vegetation observations and vegetation dynamics models.

For instance, Albergel et al. (2010) assimilated observations of LAI and surface soil moisture (SSM) within an LSM. The joint assimilation of SSM and LAI was tested at the local scale in western France and showed a positive impact on the estimation of carbon, water, and heat fluxes. Barbu et al. (2011) developed an LSM to simulate photosynthesis processes, surface carbon fluxes, and vegetation biomass and jointly assimilated soil moisture and LAI data. In another study by Albergel et al. (2017), a global land data assimilation system (LDAS-Monde) was applied over Europe and the Mediterranean basin to improve land surface variable estimation when SSM and LAI satellite-derived observations were assimilated using a Simplified Extended Kalman Filter. LDAS-Monde was more effective in estimating soil moisture in the top-soil layers, but model sensitivity to SSM decreased with depth and had almost no impact below 60 cm. Kumar et al. (2019) conducted an experiment for assessing the impact of assimilating satellite-based LAI using an Ensemble Kalman Filter over the Continental U.S. (CONUS) in the Noah-MP LSM. Results demonstrated that LAI DA has a beneficial impact on the simulation of key water budget terms (i.e., soil moisture, evapotranspiration, terrestrial water storage, and streamflow) and carbon fluxes (i.e., gross primary production and net ecosystem exchange) when compared to a large suite of ground-based reference datasets. Ling et al. (2019) assimilated Global Land Surface Satellite (GLASS) LAI data using an Ensemble Adjustment Kalman Filter technique globally. Results showed that the assimilation was able to reduce the bias in the LAI especially in low-latitude regions (from 5 m^2/m^2 to $\pm$ 1 m^2/m^2). Another recent work by Rajib et al. (2020) assimilated MODIS LAI data across eastern Iowa in the United States and showed improvements in the estimation of root zone soil moisture and water quality indicators.

This work builds upon these past studies, while also introducing several novelties. First off, it investigates the impacts of assimilating phenology observations in a land data assimilation system when the precipitation input data are strongly (either positively or negatively) biased. This is particularly crucial for assessing the hydrological conditions in data poor regions like Africa and South Asia, where precipitation information relies on satellite-based and model re-analysis products, which are well known to be affected by severe biases (Koutsouris et al., 2016, Singh and Xiaosheng 2019, Steinschneider et al., 2019). For instance, Ghatak et al. (2018) showed biases up to 70% in a suite of precipitation datasets (both satellite-based and model re-analyses) that were compared to a gauge-based product across South Asia. Yoon et al. (2019) compared ten different satellite-based and re-analysis precipitation datasets across High Mountain Asia and found average biases of 20%.

Second, this work investigates the efficiency of DI as the data assimilation approach (i.e., the LAI model state is directly replaced by observations whenever the latter become available). Although a very simple method, DI does not require any unbiasedness assumptions to operate in an optimal mode, as opposed to more sophisticated techniques such as Kalman Filters. Since biases in atmospheric forcing (and precipitation in particular) are often large and unknown (blind bias) in data-poor regions, DI represents a unique approach to assess the potential of improving the estimation of land surface variables by assimilating vegetation observations. Being the first attempt to assimilate LAI using DI under strongly biased precipitation input, this work presents a synthetic (and therefore fully controlled) experiment across CONUS to assess the potential of such approach.

2. Methodology

This study proposes an Observing System Simulation Experiment (OSSE) to better understand and quantify the Noah-MP model response to assimilating LAI information using DI. The experiment focuses on CONUS (from 25^0N, 125^0W to 53^0N, 67^0W; Fig. 1) during 2011–2015. The NASA Land Information System framework (LIS; Kumar et al., 2006), which includes several land surface models and a data assimilation system, has been used in this experiment and Noah-MP, described in detail in Section 2.1, is chosen as the LSM.

2.1. Noah-MP

The Noah-MP model has a semi-tile sub grid scheme in which the canopy layer is separated from the land surface (Niu et al., 2011). The shortwave radiation transfer is computed over the entire grid cell, while longwave radiation, latent heat, sensible heat, and ground heat fluxes are computed separately over two tiles: a fractional vegetated area (F_{veg}) and a fractional bare ground area ($1 - F_{veg}$). Multiple options are available in Noah-MP for surface water infiltration, runoff, groundwater transfer and storage, dynamic vegetation, canopy resistance, and frozen soil physics (Niu and Yang, 2007). Specifically, the prognostic

vegetation growth combines a Ball-Berry photosynthesis-based stomatal resistance (Ball et al., 1987) with a DVM (Dickinson, 1983) that allocates carbon to various parts of vegetation (leaf, stem, wood, and root) and soil carbon pools (fast and slow).

In our experiment, Noah-MP is forced with the North American Land Data Assimilation System – second phase (NLDAS-2; Xia et al., 2012). NLDAS-2 is an upgraded version of the first phase of the multi-institution NLDAS-1 (Mitchell, 2004) project, which was initiated to provide coupled atmosphere–ocean-land models with reliable initial land surface states for improving weather predictions (Xia et al., 2012). It has a time window of 40 years (1979-present), 1/8° spatial resolution, and hourly temporal resolution. Noah-MP is spun up for 30 years (1981–2010) and run at a 15-min time step. Model daily output are considered in this study.

2.2. The observing system simulation experiment

Synthetic experiments (e.g., OSSEs) are useful to quantitively assess the potential impact of land data assimilation systems before they are developed and deployed (Hoffman and Atlas 2016). OSSEs are mostly designed to investigate data assimilation ideas and have the advantage of being controlled experiments in which the reference (or 'truth') is known. In an OSSE, the observations are simulated by a model, rather than being real observations (Masutani et al., 2010). Such observations are drawn from a perturbation-free run (the Nature Run, NR), which serves as the baseline simulation (commonly referred to as 'synthetic truth') to which the output from all the other runs are compared to.

Similarly, in our experiment, described by the framework in Fig. 2, the output from the NR, which is forced with the original (unperturbed) NLDAS atmospheric forcing dataset, is considered as the synthetic truth (in terms of not only LAI, but also for all the other water, carbon, and energy variables of interest). In order to produce the 'synthetic observations', the LAI output from the nature run (NR-LAI) is aggregated to daily scale and perturbed by a multiplicative random error model (with zero mean and a standard deviation of 0.1) to mimic the uncertainties associated with real observations. This is a simplistic way of representing such uncertainties and more complex error models (e.g., seasonally dependent) could be investigated in future studies that make use of actual satellite products.

Next, two sets of open-loop (OL) simulations (i.e., no assimilation) are run by perturbing the NLDAS-2 precipitation to half and double of the original NLDAS-2 data to generate two extreme cases, the one in which NLDAS-2 has a dry bias and the one in which NLDAS-2 has a wet bias. This is obtained by multiplying the precipitation input by a constant scaling factor, i.e., 0.5 and 2.0, for creating the dry and wet conditions, respectively. Such simple multiplicative error model assumes that the given dataset has perfect detection (neither false alarms nor missed events), i.e., no-rain (rainy) pixels will remain no-rain (rainy) pixels in the perturbed forcing dataset. This is a strong assumption for re-analysis precipitation (and for satellite-based products as well), which are well known to be affected by detection errors. Nevertheless, a series of articles by Maggioni et al. (2011, 2012, 2013) showed minimal improvement in soil moisture simulations when a more complex precipitation error model (that simulates both false alarm and missed events) was considered in a land data assimilation system. Thus, a simple error characterization is chosen for this study, but future work should investigate this issue further.

Finally, two data assimilation (DA) runs (wet and dry) are performed by directly replacing the LAI model state with observations obtained by the perturbed NR-LAI. In a DI DA, the observation is fully trusted (Kumar et al., 2008) and model estimates are replaced by the observations whenever the latter are available (Reichle, 2008). In this case the model is replaced by the synthetic LAI observations every day at 1:00 am. DI, one of the simplest data assimilation methods, was chosen in this experiment mainly because it does not require any unbiased model or observation. Furthermore, DI is computationally efficient and easy to implement, as the updating algorithm does not account for system dynamics or measurement statistics (Walker et al., 2003). In the past, DI has been successfully used to assimilate snow cover, freeze/thaw state, soil moisture, surface albedo in land surface models, as well as radiances in aerosols transport models (Alavi et al., 2010, Kumar et al., 2020, Liston et al., 1999, Sun, 2004,Weaver et al., 2007, Xue et al., 2019). In this work, we propose to apply the same concept to vegetation data, by not only updating LAI, but also the modeled leaf biomass, computed by dividing the LAI value by the specific leaf area. The root mass and stem mass are not updated in this experiment.

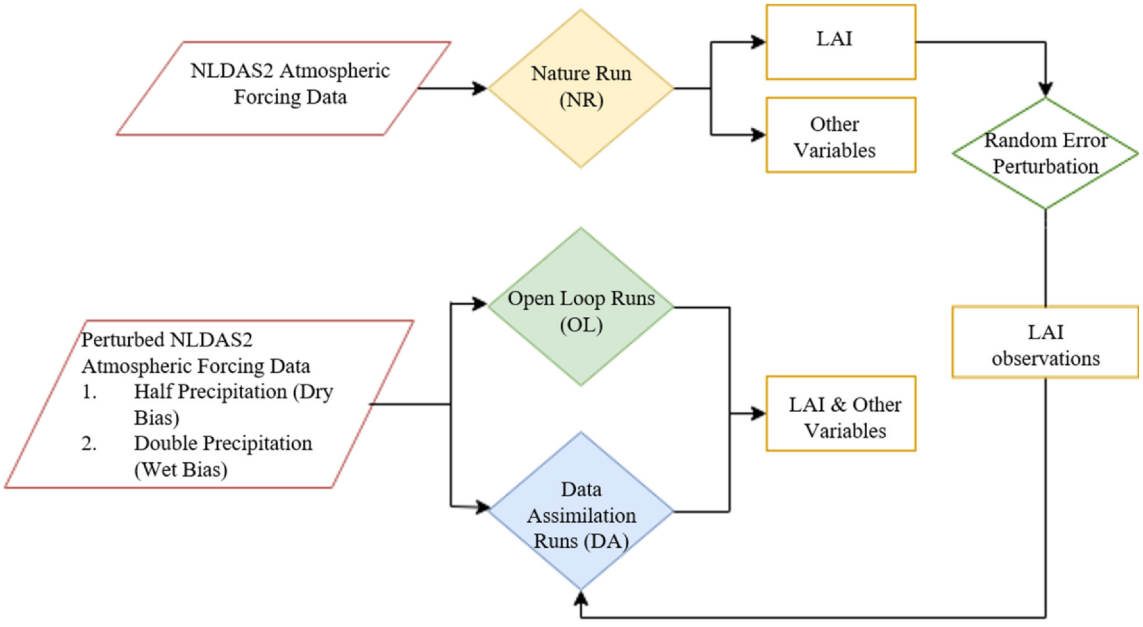

Fig. 2. Schematic diagram of the experimental setup. Parallelograms represent input data, rhombi represent models/simulations, and rectangles represent output variables.

Table 1
List of variables with corresponding acronyms and units.

Variable	Acronym	Unit
Surface Soil Moisture	SSM	m^3/m^3
Rootzone Soil Moisture	RZSM	m^3/m^3
Intercepted Liquid Water	ILW	mm
Total Evapotranspiration	ET	kg/m^2s
Net Ecosystem Exchange	NEE	g/m^2s
Short Lived Carbon in Shallow Soil	CSS	g/m^2
Canopy Sensible Heat	CSH	W/m^2
Surface Soil Temperature	SST	K

2.3. Evaluation variables and metrics

Daily water, carbon, and energy variables (listed in Table 1) from the OL and DA output for both wet and dry conditions are compared to the corresponding "true" output from the NR run. In terms of water variables, we consider: surface soil moisture (SSM; m^3/m^3), defined in Noah-MP as the water content in the top 10 cm of the soil column; rootzone soil moisture (RZSM; m^3/m^3), defined as the water content in the top 100 cm of soil; intercepted liquid water (ILW; mm), defined as the amount of precipitation that does not reach the soil, but that instead gets absorbed by canopy, plants, and forest floor; and total evapotranspiration (ET; kg/m^2s), defined as the total amount of water released to the atmosphere from land and plant. As carbon and energy variables, we select: net ecosystem exchange (NEE; g/m^2s), defined as the amount of carbon exchange between plant and atmosphere; short-lived carbon in shallow soil (CSS; g/m^2), defined as the short-lived carbon pool, which is the summation of total leaf and root turnover and total amount of dead leaf; canopy sensible heat (CSH; W/m^2), defined as the total amount of heat transferred to the air from ground and vegetation; and surface soil temperature (SST; K), defined as the temperature of the soil in the top 10 cm.

Two performance metrics are considered: the relative bias (RB) and the normalized unbiased root mean square error (NUbRMSE). Metrics are computed at each grid cell separately for all the experiments (OL and DA) during the 5-year study period. RB is an estimate of the systematic error and defined here as the normalized difference between the estimated value (either from OL or DA) and the reference NR variable:

$$RB = \frac{\frac{\sum(\hat{x} - X_{NR})}{N}}{\frac{\sum(X_{NR})}{N}} * 100\% \quad (1)$$

where $\hat{x}$ represents the output variable from either OL or DA runs (either from dry or wet conditions), X_{NR} is the corresponding NR variable, and N is the number of days.

In order to investigate the random error alone, we use the NUbRMSE, following the definition of Bhuiyan et al. (2018), Falck et al. (2018), and Zhang et al. (2020), in which we first remove the bias from the OL and DA output variables and then normalize by the reference (i.e., NR values):

Table 2
Relative bias (%) between output variables from the OL (or DA) run and output variables from the NR averaged across CONUS for both dry and wet conditions. The difference (%) between DA and OL is also reported.

	Dry condition			Wet condition		
	OL	DA	|OL|-|DA|	OL	DA	|OL|-|DA|
SSM	−11.0	−12.0	−1.00	9.30	9.50	−0.20
RZSM	−10.3	−11.7	−1.40	8.80	9.30	−0.50
ILW	−44.7	−28.7	16.0	83.1	35.6	47.5
ET	−29.9	−28.2	1.70	28.9	26.0	2.90
NEE	90.5	57.6	32.9	−110	−50.2	60.2
CSS	−1.80	−1.00	0.80	1.70	0.50	1.20
CSH	0.10	19.3	−19.2	−2.80	−11.1	−8.30
SST	0.20	0.10	0.10	−0.20	−0.10	0.10

Table 3
Same as in Table 2 but for NUbRMSE (%).

	Dry condition			Wet condition		
	OL	DA	|OL|-|DA|	OL	DA	|OL|-|DA|
SSM	6.87	7.08	−0.21	7.22	7.44	−0.22
RZSM	6.55	7.32	−0.77	6.76	6.93	−0.17
ILW	154	106	48.0	335	166	169
ET	48.9	47.5	1.40	63.2	61.5	1.70
NEE	133	79.8	53.2	176	91.0	85.0
CSS	1.31	0.72	0.59	1.18	0.41	0.77
CSH	43.2	29.8	13.5	42.8	22.6	20.2
SST	0.41	0.33	0.08	0.50	0.50	0.00

$$NUbRMSE = \frac{\sqrt{\frac{\sum\left(\left(\left(\hat{x} - \frac{\sum(\hat{x})}{N}\right) - \left(X_{NR} - \frac{\sum(X_{NR})}{N}\right)\right)^2\right)}{N}}}{\frac{\sum(X_{NR})}{N}} * 100\% \quad (2)$$

Normalized metrics allow for easier comparison among variables of different nature and units. In this work, both RB and NUbRMSE are shown as percentage values and computed for every model pixel across the study area.

3. Results

Changes in LAI due to DA (with respect to the corresponding OL run) are shown in Fig. 3. In the dry condition, the application of DA introduces additional vegetation to the system to balance the negative bias in the input precipitation. In other words, the model tends towards the dry side, but the observations see more vegetation than the one estimated by the model, whereas the wet condition case shows the exact opposite (i.e., lower LAI in the DA run). Both in the dry and wet condition, the central part of CONUS is particularly impacted by LAI DA. Some areas over the eastern part of CONUS also show large changes due to the application of LAI DA. Such areas mainly correspond to

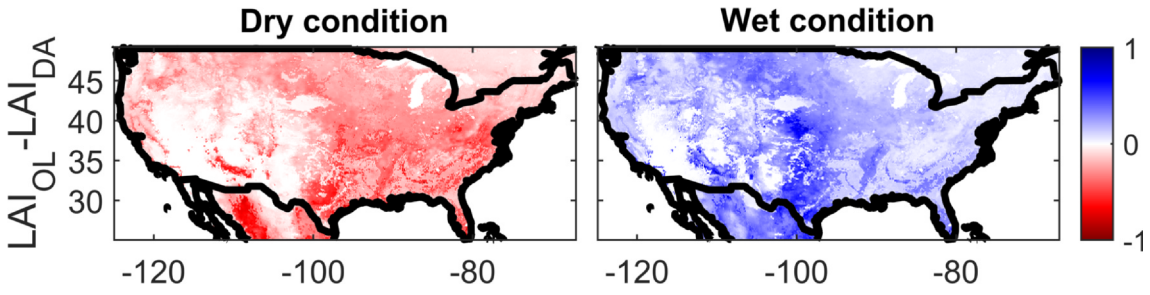

Fig. 3. Difference in LAI simulated by the OL and DA runs for dry (left) and wet (right) conditions. Red (blue) indicates an increase (decrease) in LAI due to the DA of LAI. (For interpretation of the references to colour in this figure legend, the reader is referred to the web version of this article.)

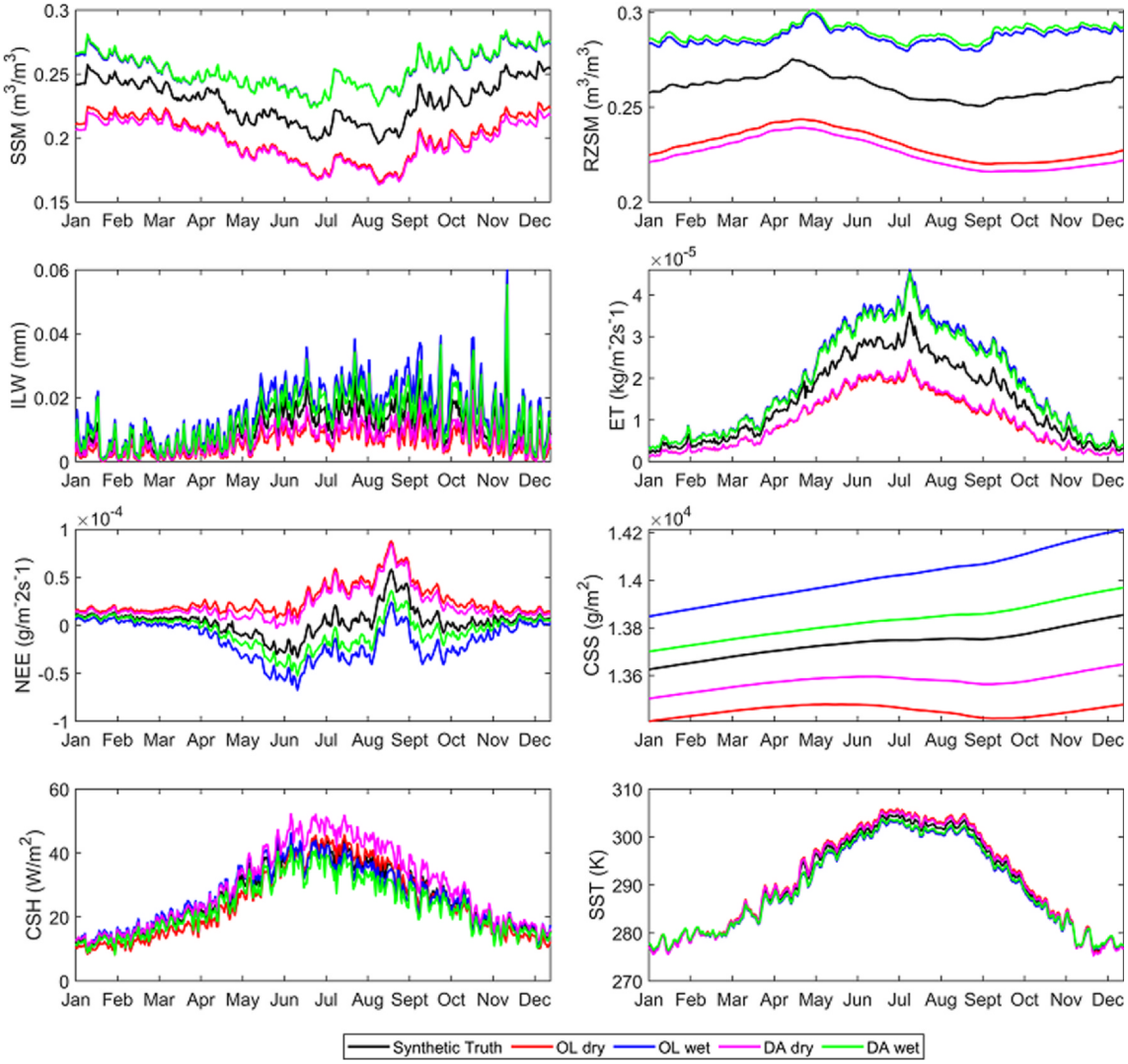

Fig. 4. Time series of water, carbon and energy variables averaged over CONUS from the NR, OL, and DA runs during 2013 and for both dry and wet condition experiments.

shrublands and croplands (Fig. 1). This is due to the fact that plants characterized by smaller roots are more affected by precipitation, whereas plants with longer roots (i.e., woodlands and forests) are more resistant to changes in precipitation, because they can pull water from the deeper layer of the soil.

The overall systematic and random errors of the eight variables simulated by the OL (or DA) runs with respect to the reference NR output are computed for both wet and dry conditions. RB and NUbRMSE are averaged across CONUS and presented in Tables 2 and 3, respectively, together with differences between the OL and DA runs, which highlight whether DA improves (positive sign) or worsens (negative sign) the corresponding OL run. SSM, RZSM, and CSH show a degradation (with respect to the OL) in the average RB after LAI is assimilated under, with larger degradation under dry condition. Similarly, LAI DA worsens the NUbRMSE of soil moisture, with a larger degradation in the dry condition for RZSM, but with no difference between dry and wet condition for SSM and an improvement in CSH. On the other hand, ILW, ET, NEE, and CSS improve after the application of LAI-DA in terms of both systematic and random error, with a consistently higher improvement in the wet condition compared to the dry condition, with the exception for SST whose statistics only slightly change after the implementation of the LAI DA scheme.

In order to further investigate these overall performances, we investigate time series during one selected year (i.e. 2013) for averages of all select variables across CONUS. We also assess the spatial variability of the improvement/degradation in the evaluation metrics introduced in Section 2.3, by showing maps of differences in RB and NUbRMSE. As a last analysis, we explore the dependency of the model performance as a function of four main vegetation covers (Forest and woodland, Shrubland, Grassland, and Cropland). Results are presented in sub-section 3.1 for the water variables (SSM, RZSM, ILW, and ET) and in sub-section 3.2 for the carbon and energy variables (NEE, CSS, CSH, and SST) and further discussed in Section 4.

3.1. Water variables

As shown in the time series in Fig. 4, DA pushes the modeled SSM and RZSM in the opposite direction with respect to the NR, degrading the original (OL) model simulation. This is corroborated by the maps of RB and NUbRMSE differences in Figs. 5 and 6, respectively, presenting a clear degradation in soil moisture (both SSM and RZSM) in several regions of the continental US. Nevertheless, some other areas do show an improvement thanks to DA, e.g., SSM RB in the southeastern US under wet condition. Overall, the degradation in soil moisture is consistently less pronounced under wet condition. In the dry experiment, Noah-MP is fed by only half of the NLDAS-2 precipitation and there is

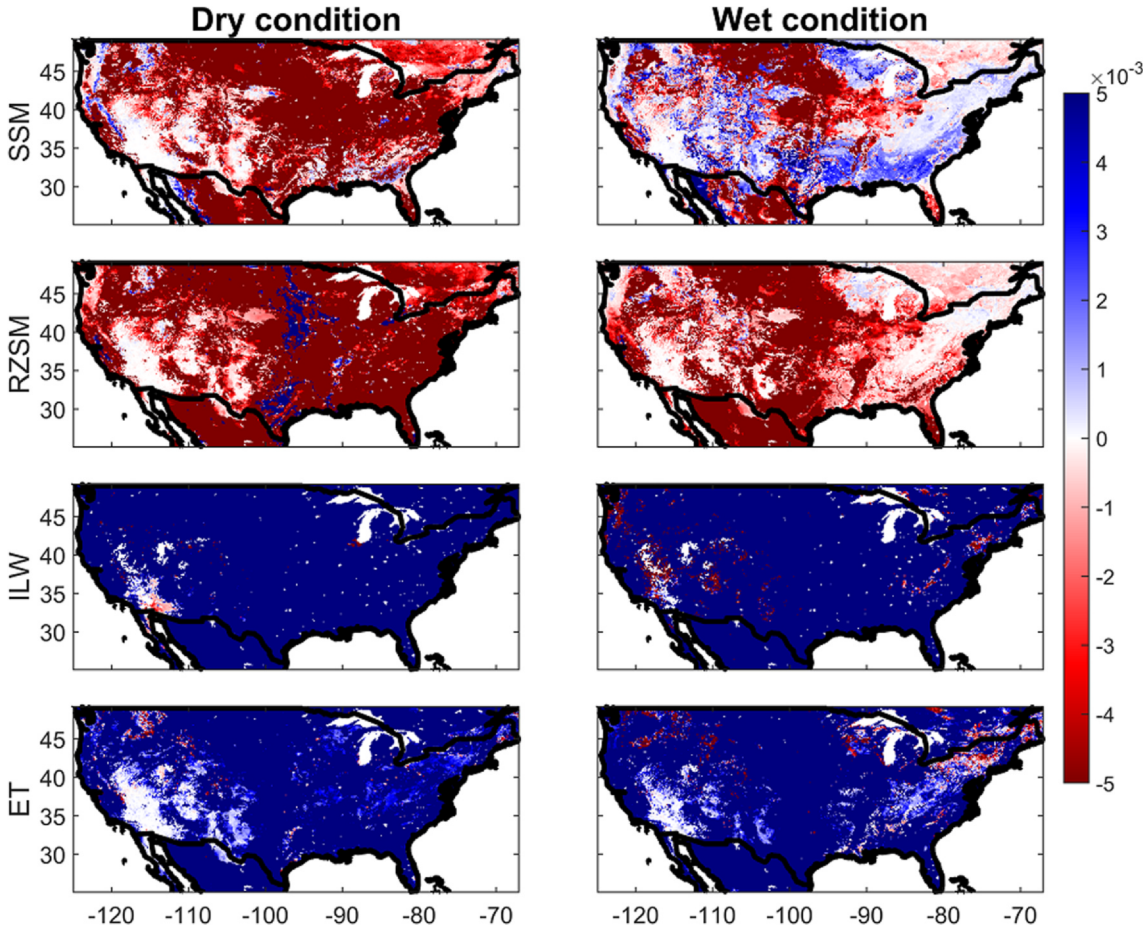

Fig. 5. Change in the RB (difference between the DA run and the OL run) for the four water variables for dry and wet conditions across CONUS during 2011–2015. Blue (red) color indicates improvement (degradation) after DA with respect to the NR output variables. (For interpretation of the references to colour in this figure legend, the reader is referred to the web version of this article.)

no additional water source. LAI DA introduces more vegetation to the system and that results in more water absorption, which worsens the estimation of soil moisture. On the contrary, in the wet condition experiment, precipitation is doubled, adding more water to the system. When the soil saturates, soil moisture reaches its maximum value and no longer changes, which translates into smaller variability in soil moisture under the wet condition compared to the dry condition experiment.

As shown by the time series in Fig. 4 and more clearly by the maps in Figs. 5 and 6, the DA simulations of ILW and ET improve compared to their corresponding OL runs, moving them towards the synthetic truth. A decrease in RB is evident across CONUS for both variables and under both precipitation bias conditions (Fig. 5). However, some locations in the south and northeastern US, present a degradation in NUbRMSE (Fig. 6) in the dry and wet condition experiments, showing that the LAI DA cannot correct for the random error in all cases.

Fig. 7 summarizes the performance of the proposed DA scheme as a function of land cover. In general, LAI DA degrades soil moisture but improves ILW and ET across all vegetation covers under wet and dry conditions and in terms of both systematic and random errors. For SSM, ILW, and ET, forest and woodland areas are less impacted by the LAI DA compared to the other vegetation covers. Forest and woodland regions have vegetation with deeper roots, while shrubland, grassland, and cropland are characterized by plants with shallower roots. The lack of rain (dry condition experiment) makes the plants with smaller roots dry out and die, whereas plants with longer roots can still survive by pulling water from the deeper soil (Bonan, 2002). Thus, LAI DA does not have a strong impact on water variables in forest and woodland areas, although it does in other regions like the Great Plains. RZSM in the dry condition and in forest and woodland areas shows a larger impact compared to other variables, because long rooted plants would pull even more water from the rootzone, while precipitation is reduced.

3.2. Carbon and energy variables

All four carbon and energy variables (NEE, CSS, CSH, and SST) present an overall improvement after the application of DA in terms of RB and NUbRMSE (Tables 2 and 3). Fig. 4 shows how NEE and CSS are consistently pushed towards the NR by the DA scheme during the whole year. Specifically, NEE decreases in June-July, when the LAI is the highest, which indicates less carbon in the atmosphere and more vegetation on the ground. CSS presents an increasing trend, which demonstrates that total amount of living carbon in the soil increases over during the year, especially after fall when the leaf and root turnover is the highest. However, DA-CSH has a noticeable degradation during summer under both dry and wet condition. Differences between OL-SST and DA-SST are minimal (as already highlighted in Tables 2 and 3). with an improvement during the summer. OL-SST is higher than the NR during the summer in the dry run and vice versa in the wet run (Fig. 4). This happens because a decrease (increase) in vegetation, which is due to less (or more) precipitation in the model input, increases (decreases) soil temperature. SST-DA shows slight degradation in the winter, when vegetation is less abundant and soil temperature depends not only on air temperature, but also on SSM, which degrades after the application of LAI-DA.

Figs. 8 and 9 confirm the overall improvement in the selected

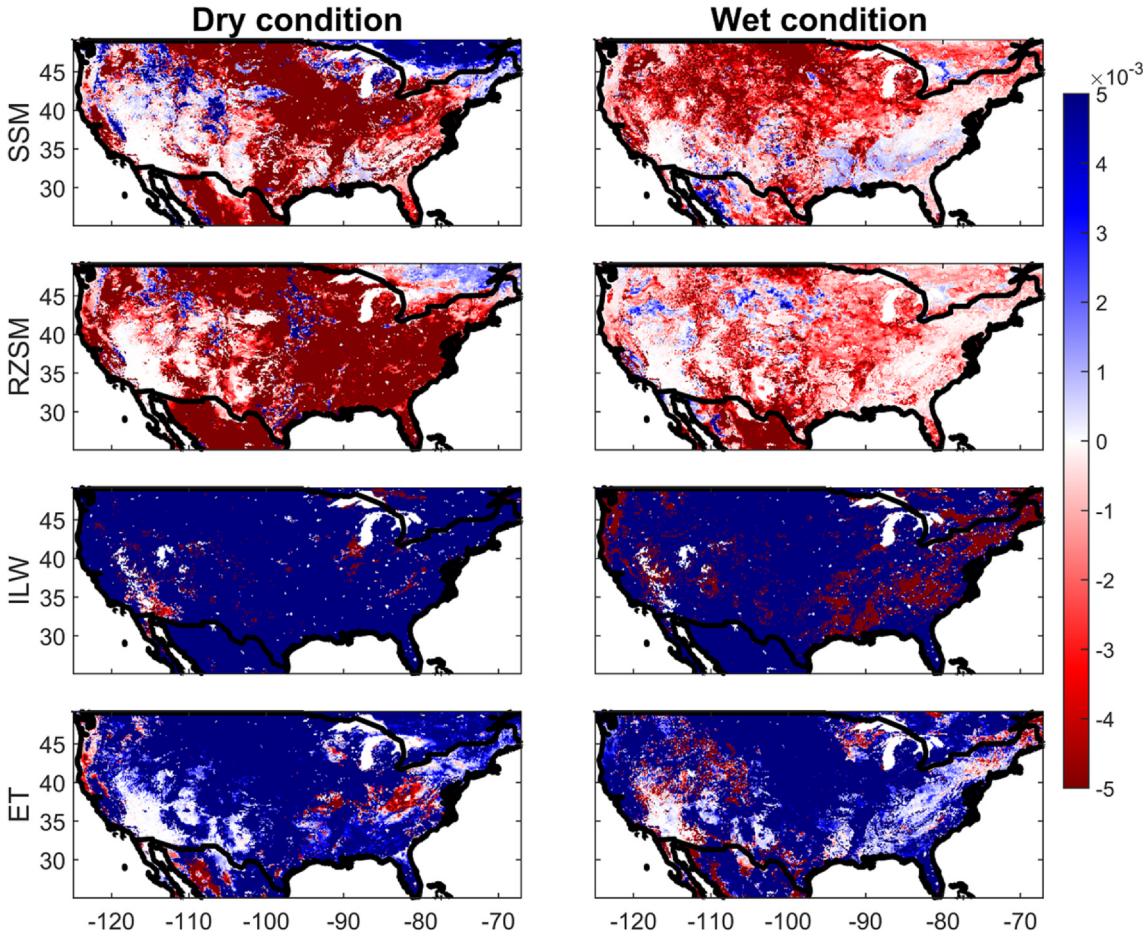

Fig. 6. Same as in Fig. 5 but for NUbRMSE.

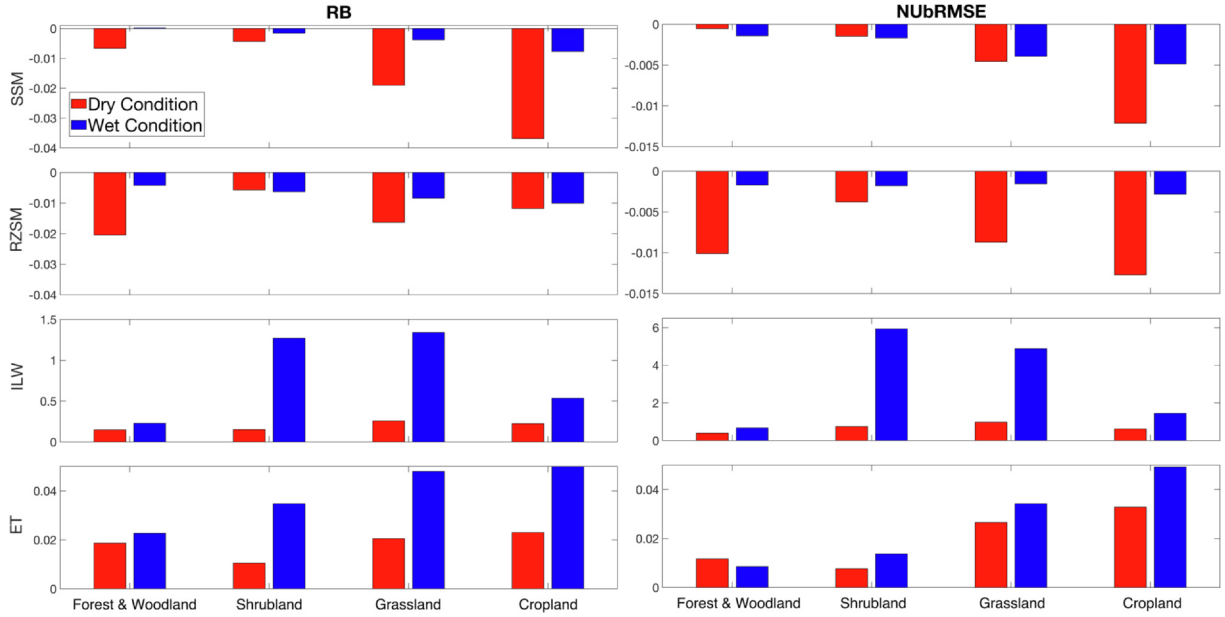

Fig. 7. Difference in RB (left) and UbRMSE (right) between the OL run and corresponding DA run across different vegetation covers (Forest and Woodland, Shrubland, Grassland, and Cropland) during 2011–2015 for all the water variables. Positive (negative) values correspond to an improvement (degradation) thanks to DA.

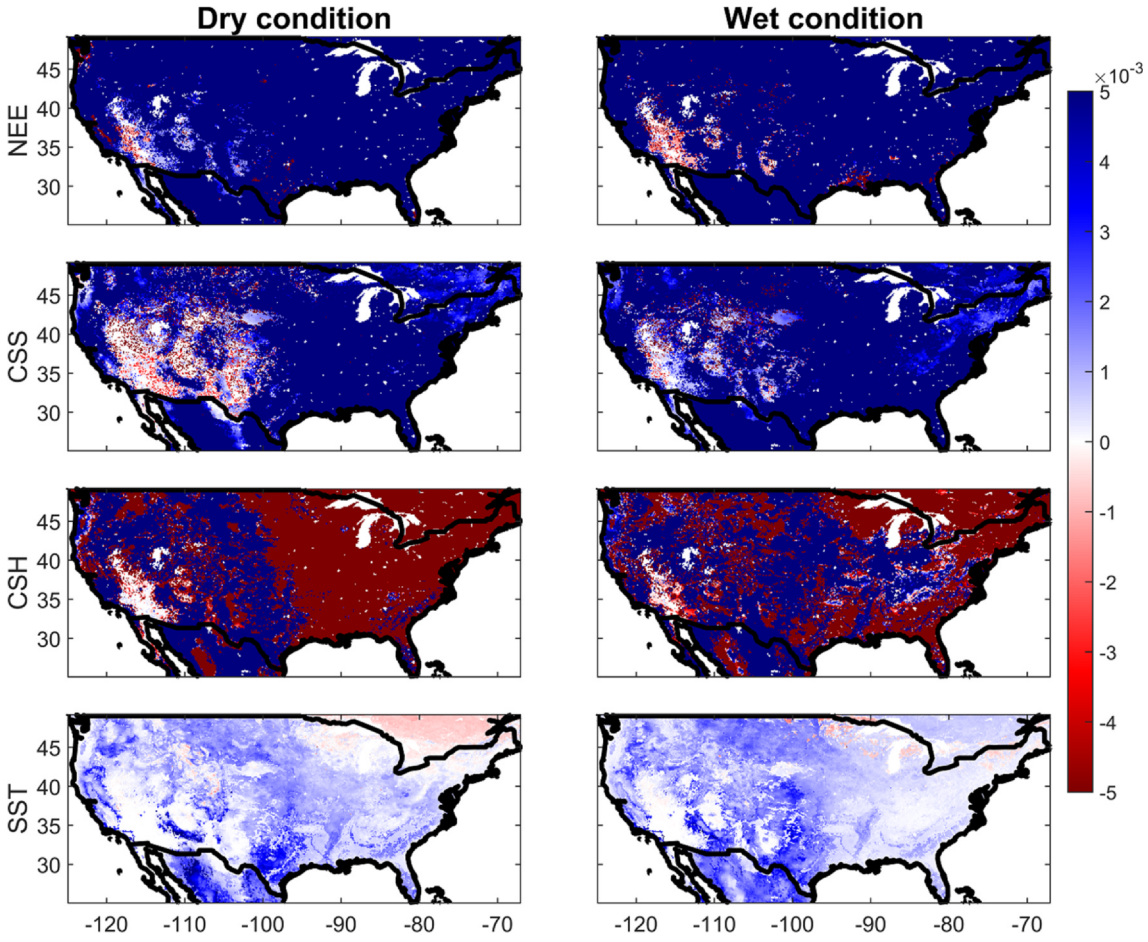

Fig. 8. Change in the RB (difference between the DA run and the OL run) for the four carbon and energy variables for dry and wet conditions across CONUS during 2011–2015. Blue (red) color indicates improvement (degradation) after DA with respect to the NR output variables. (For interpretation of the references to colour in this figure legend, the reader is referred to the web version of this article.)

carbon and energy variables. However, RB seems to increase after DA in a region in the Southwestern US and the NEE NUbRMSE has a similar behavior in some areas in the northeastern and northwestern US. CSH shows a degradation in RB in both dry and wet experiments over the eastern and central part of US, but an improvement in NUbRMSE almost all over CONUS. Such degradation in CSH corresponds to the same locations where soil moisture shows the largest degradation after DA. As highlighted in section 2.3, CSH is the combined heat flux from ground and vegetation to the atmosphere, with the ground-to-air heat flux being the dominant factor (Bonan, 2002). The heat flux from the ground is highly correlated with the soil water content, which is part of the reason why CSH worsens after DA (Hwang, 1985, Guan et al., 2009).

The change in SST once again is minimal, with some regions showing no change between the OL and DA runs, and some others presenting a slight improvement or a slight degradation. This latter is only evident in the NUbRMSE under wet condition and specifically over forest/woodland and cropland areas (as demonstrated in Fig. 10). DA in wet condition reduces the vegetation amount modeled by Noah-MP, which would bring SST up. However, in the northern part of the US SST is more affected by air temperature, rather than the surface condition. In forest/woodland and cropland areas, all the variables show an improvement after the application of LAI-DA, except for CSH in the dry condition, (Fig. 10). For all the carbon and energy variables forest and woodland areas are the least impacted after the application of DA, just like for the water variables.

4. Discussion

In the proposed OSSE, we assimilate daily synthetic observations of LAI that mimic temporally smoothed MODIS observations, commonly available every 8 days. Obtaining satellite observations at such frequency is challenging due to frequent cloud coverage during winters. Thus, the proposed experiment and associated results should be considered as a best-case scenario in which LAI observations are consistently available every 8 days. Assimilating observations every 8 days may cause instability in the model dynamics, so an alternative approach is proposed here to interpolate between observations and update the model state more often (i.e., every day).

When actual satellite-based LAI observations are assimilated in the LSM and ground-based measurements are used as reference for validation purposes, the LAI DA performance may differ to the one presented in the results section, and what looks like a degradation in the OSSE may be an improvement in the actual data experiment. For instance, in this experiment, the LAI DA could not largely improve the RB and NUbRMSE associated with surface and root zone soil moisture, but this may be different if real satellite products are merged within an LSM, especially in irrigated fields that are not modeled within the current Noah-MP framework. As a matter of fact, Kumar et al. (2019) show an improvement not only in ET, but also in RZSM thanks to the assimilation of satellite-based LAI within a LSM using an Ensemble Kalman Filter across the central plains in US, mainly characterized by crops. Future work should therefore analyze LAI-soil moisture feedback in the model simulations during different seasons to illustrate why LAI assimilation degrades soil moisture estimates in some regions. This

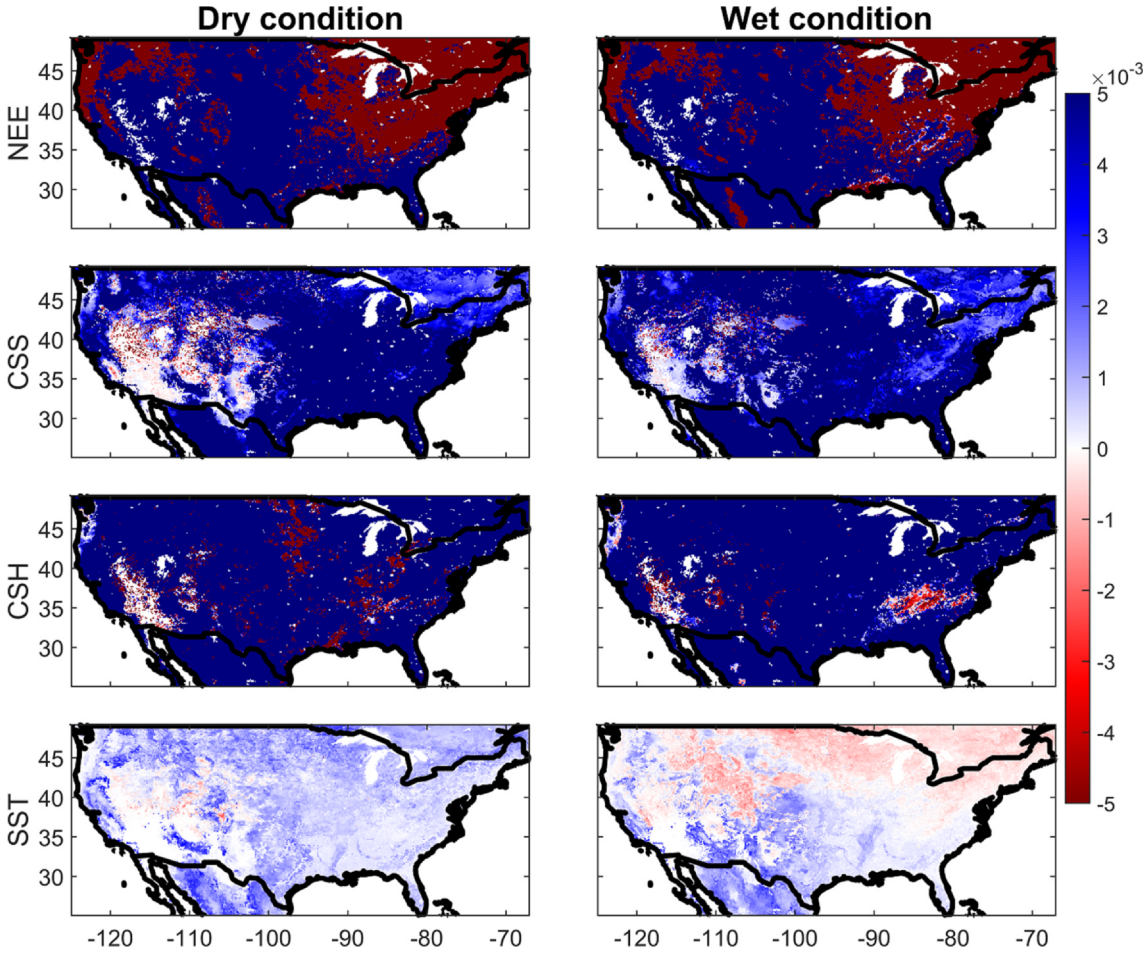

Fig. 9. Same as in Fig. 8 but for NUbRMSE.

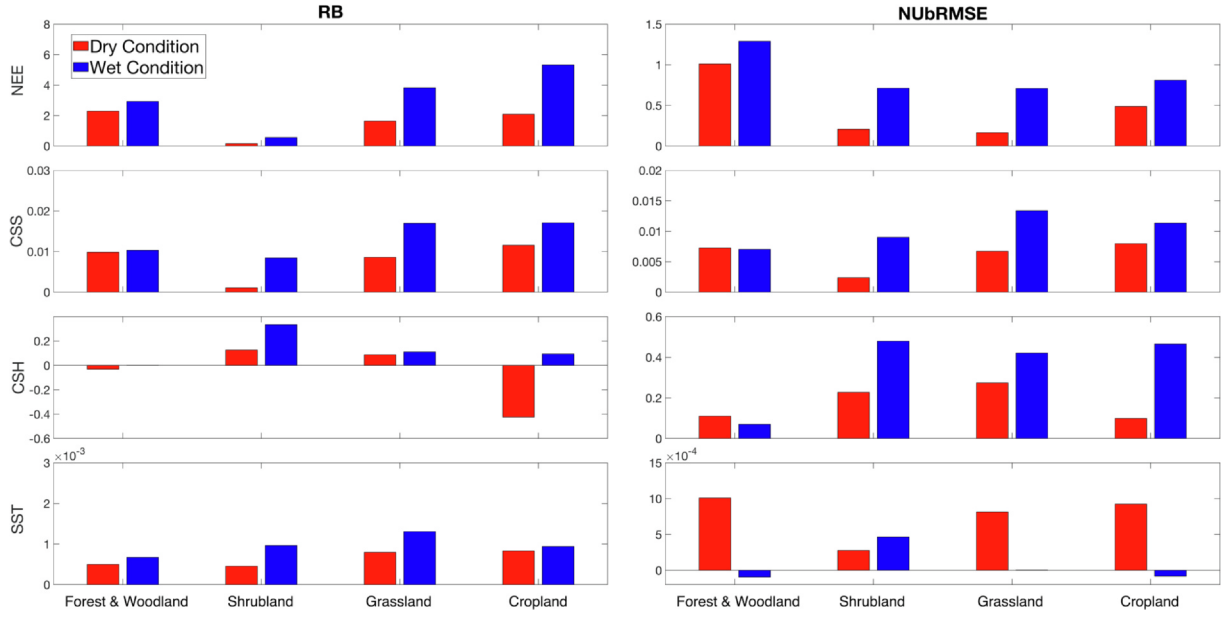

Fig. 10. Difference in RB (left) and UbRMSE (right) between the OL run and corresponding DA run across different vegetation covers (Forest and Woodland, Shrubland, Grassland, and Cropland) during 2011–2015 for the carbon and energy variables. Positive (negative) values correspond to an improvement (degradation) thanks to DA.

would be particularly useful for future ecohydrology data assimilation studies.

Systematic errors (quantified by RB) are reduced thanks to LAI DA for most variables considered in this study (except for SSM, RZSM, and CSH) in both dry and wet condition experiments and across the whole study area. In terms of random errors (NUbRMSE), DA improves most of the variables for both wet and dry conditions except the SSM and RZSM, with some regions also showing a degradation in NEE. Similarly, the work by Kumar et al. (2019) mentioned above shows an improvement in NEE, except in the Northwestern region of the US and areas around the Great Lakes. In general, the improvement in both RB and NUbRMSE is larger when the precipitation forcing has a positive bias (wet condition) than in the dry condition experiment. This is because, in the latter case, the amount of water available in the system is limited, but the assimilation of LAI observations introduces vegetation, which causes more root water uptake from the soil and worsens the soil moisture estimation.

In the OSSE proposed here, some water variables (e.g., ET and ILW) show an improvement both in dry and wet bias conditions, though the improvement under dry biases is marginal. These results corroborate what shown in the work recently published by Zhang et al. (2020), who performed an OSSE at the global scale to assimilate LAI with an Ensemble Kalman Filter technique and observed only marginal improvements in soil moisture contents, a degradation in SSM under dry precipitation conditions, and significant improvements in ET in wet bias conditions.

Furthermore, we evaluate the LAI-DA impact on carbon and energy variables, most of which (except CSH), improve across the entire domain under both wet and dry bias conditions. Results show that croplands, grasslands, and shrublands are the most impacted by the application of LAI DA (as highlighted in Figs. 7 and 10), as plants with smaller roots are more affected by precipitation (which is perturbed in the OL and DA simulations), while plants with longer roots (that characterize woodlands and forests) can pull water from the deeper soil and are therefore more resistant to changes in precipitation. This also aligns with the findings by Zhang et al. (2020) who showed a larger impact of the LAI DA in regions characterized by short root plants when compared to forests and woodlands.

In summary, DI of LAI can improve almost all the carbon and energy variables under both wet and dry conditions and across different vegetation covers. Nevertheless, the proposed DA scheme was not able to improve surface and rootzone soil moisture. Soil moisture plays a fundamental role in land surface processes and in the water, carbon, and energy cycles, as it i) controls the partitioning of the energy incident on the land surface; ii) is a storage component for precipitation and radiation (and therefore impact cloud formation, precipitation, runoff, and evapotranspiration); and iii) governs several feedbacks at the local, regional, and global scale (e.g., soil moisture-temperature and soil moisture-precipitation). Previous work on the joint assimilation of LAI and soil moisture observations has shown promising improvements in both water and carbon dioxide fluxes (Albergel et al., 2010, Albergel et al., 2017, Barbu et al., 2011, and Bonan et al., 2019). However, these studies have only focused on limited domain or for a specific crop type. Thus, future research work should look at dual assimilation methods that merge different types of observations (e.g., surface soil moisture and LAI) if the goal is to improve land surface processes as a whole.

5. Conclusions

This work proposes a synthetic experiment to investigate the impact of assimilating LAI observations within a land surface model through DI. The experiment is performed across the continental US during a 5-year time period (January 2011-December 2015), adopting the Noah-MP LSM forced with NLDAS-2 meteorological forcing data. The efficiency of LAI DA is investigated in terms of several water, carbon, and energy states and fluxes under strongly (both negatively and positively) biased precipitation forcing. Although DI is a very naïve DA approach, it does not require any unbiasedness assumptions to optimally operate (as opposed to the more sophisticated Kalman Filter), which is critical since biases in atmospheric forcing (and precipitation in particular) are often large and unknown.

In summary, this study demonstrates how assimilating LAI observations through the simplest DA method available (i.e., direct insertion) has the potential to improve LSM estimation of some water (e.g., ILW), carbon (e.g., NEE), and energy (e.g., SST) variables. These improvements are often a function of the land cover, as demonstrated in this work. Thus, future work should be directed towards a more in-depth investigation of such dependence to identify what vegetation types would gain the most from assimilating LAI observations. However, as results from this study demonstrate that soil moisture variables would not benefit from the assimilation of LAI alone, the combined assimilation of both LAI and surface soil moisture observations should also be explored.

This work opens new research directions as real observational data (e.g., MODIS and GLASS products) available globally could be assimilated in the proposed DA framework, which could then be expanded to the global scale and benefit several regions of the world where ground monitoring of water, energy, and carbon states and fluxes is limited but extremely important (e.g., Amazon forest, High Mountain Asia). The efficiency of the proposed DI that adopts a simple multiplicative precipitation error model should be also compared to more sophisticated techniques (e.g., Ensemble Kalman Filter) and more complex precipitation error models that simulate false alarms and missed events in the original products.

Declaration of Competing Interest

The authors declare that they have no known competing financial interests or personal relationships that could have appeared to influence the work reported in this paper.

Acknowledgements

This work was supported by the NASA Modeling, Analysis, and Prediction Program (MAP) program (award number 80NSSC17K0109). All the model computations were run using the ARGO cluster, administered by the Office of Research Computing at George Mason University, VA (http://orc.gmu.edu).

Author contribution

A. R. performed all analyses and wrote the manuscript. X.Z. developed the code for the LAI data assimilation within the LIS framework. V.M. and P.H. conceptualized the experiment. S.V. and D.M. provided the LIS 7.2 version code, configuration files, and helped with mode debugging. All co-authors contributed to the interpretation of results.

References

Alavi, N., Berg, A.A., Warland, J.S., Parkin, G., Verseghy, D., Bartlett, P., 2010. Evaluating the impact of assimilating soil moisture variability data on latent heat flux estimation in a land surface model. Can. Water Resourc. J. 35 (2), 157–172. https://doi.org/10.4296/cwrj3502157.

Albergel, C., Calvet, J.-C., Mahfouf, J.-F., Rüdiger, C., Barbu, A.L., Lafont, S., Roujean, J.-L., Walker, J.P., Crapeau, M., Wigneron, J.-P., 2010. Monitoring of water and carbon fluxes using a land data assimilation system: A case study for southwestern France. Hydrol. Earth Syst. Sci. Discuss. 14, 1109–1124.

Albergel, C., Munier, S., Leroux, D.J., Dewaele, H., Fairbairn, D., Barbu, A.L., Gelati, E., Dorigo, W., Faroux, S., Meurey, C., Le Moigne, P., Decharme, B., Mahfouf, J.-F., Calvet, J.-C., 2017. Sequential assimilation of satellite-derived vegetation and soil moisture products using SURFEX_v8.0: LDAS-Monde assessment over the Euro-Mediterranean area. Geosci. Model Dev. Discuss. 1–53. https://doi.org/10.5194/gmd-2017-121.

Ball, J.T., Woodrow, I.E., Berry, J.A., 1987. A Model Predicting Stomatal Conductance and its Contribution to the Control of Photosynthesis under Different Environmental Conditions. In: Biggins, J. (Ed.), Progress in Photosynthesis Research. Springer,

Netherlands, pp. 221–224. https://doi.org/10.1007/978-94-017-0519-6_48.
Barbu, A.L., Calvet, J.-C., Mahfouf, J.-F., Albergel, C., Lafont, S., 2011. Assimilation of soil wetness index and leaf area index into the ISBA-A-gs land surface model: Grassland case study. Biogeosciences 8 (7), 1971–1986. https://doi.org/10.5194/bg-8-1971-2011.
Bhuiyan, M.A.E., Nikolopoulos, E.I., Anagnostou, E.N., Quintana-Seguí, P., Barella-Ortiz, A., 2018. A nonparametric statistical technique for combining global precipitation datasets: Development and hydrological evaluation over the Iberian Peninsula. Hydrol. Earth Syst. Sci. 22 (2), 1371–1389. https://doi.org/10.5194/hess-22-1371-2018.
Bonan, B., Albergel, C., Zheng, Y., Barbu, A.L., Fairbairn, D., Munier, S., Calvet, J.-C., 2019. An Ensemble Square Root Filter for the joint assimilation of surface soil moisture and leaf area index within LDAS-Monde: Application over the Euro-Mediterranean region [Preprint]. Hydrometeorol./Modell. Approach. https://doi.org/10.5194/hess-2019-391.
Bonan, G.B., 2002. Ecological climatology: Concepts and applications. Cambridge University Press.
Clark, D.B., Mercado, L.M., Sitch, S., Jones, C.D., Gedney, N., Best, M.J., Pryor, M., Rooney, G.G., Essery, R.L.H., Blyth, E., Boucher, O., Harding, R.J., Huntingford, C., Cox, P.M., 2011. The Joint UK Land Environment Simulator (JULES), model description – Part 2: Carbon fluxes and vegetation dynamics. Geosci. Model Dev. 4 (3), 701–722. https://doi.org/10.5194/gmd-4-701-2011.
Dai, Y., Zeng, X., Dickinson, R.E., Baker, I., Bonan, G.B., Bosilovich, M.G., Denning, A.S., Dirmeyer, P.A., Houser, P.R., Niu, G., Oleson, K.W., Schlosser, C.A., Yang, Z.-L., 2003. The common land model. Bull. Am. Meteorol. Soc. 84 (8), 1013–1024. https://doi.org/10.1175/BAMS-84-8-1013.
Dickinson, R. E. (1983). Land Surface Processes and Climate—Surface Albedos and Energy Balance. In Advances in Geophysics (Vol. 25, pp. 305–353). Elsevier. https://doi.org/10.1016/S0065-2687(08)60176-4.
Falck, A.S., Maggioni, V., Tomasella, J., Diniz, F.L.R., Mei, Y., Beneti, C.A., Herdies, D.L., Neundorf, R., Caram, R.O., Rodriguez, D.A., 2018. Improving the use of ground-based radar rainfall data for monitoring and predicting floods in the Iguaçu river basin. J. Hydrol. 567, 626–636. https://doi.org/10.1016/j.jhydrol.2018.10.046.
Ghatak, D., Zaitchik, B., Kumar, S., Matin, M.A., Bajracharya, B., Hain, C., Anderson, M., 2018. Influence of precipitation forcing uncertainty on hydrological simulations with the NASA South Asia land data assimilation system. Hydrology 5 (4), 57. https://doi.org/10.3390/hydrology5040057.
Guan, X., Huang, J., Guo, N., Bi, J., Wang, G., 2009. Variability of soil moisture and its relationship with surface albedo and soil thermal parameters over the Loess Plateau. Adv. Atmos. Sci. 26 (4), 692–700. https://doi.org/10.1007/s00376-009-8198-0.
Hoffman, R.N., Atlas, R., 2016. Future observing system simulation experiments. Bull. Am. Meteorol. Soc. 97 (9), 1601–1616. https://doi.org/10.1175/BAMS-D-15-00200.1.
Hwang, S.J., 1985. Effects of the soil moisture on the net radiation flux and soil heat flux at the ground surface. Geograph. Rev. Jpn., Ser. A, Chirigaku Hyoron 58 (1), 39–46. https://doi.org/10.4157/grj1984a.58.1_39.
Koutsouris, A.J., Chen, D., Lyon, S.W., 2016. Comparing global precipitation data sets in eastern Africa: A case study of Kilombero Valley, Tanzania: Comparing global precipitation data sets in Tanzania, East Africa. Int. J. Climatol. 36 (4), 2000–2014. https://doi.org/10.1002/joc.4476.
Kumar, S., Peterslidard, C., Tian, Y., Houser, P., Geiger, J., Olden, S., Lighty, L., Eastman, J., Doty, B., Dirmeyer, P., 2006. Land information system: An interoperable framework for high resolution land surface modeling. Environ. Modell. Software 21 (10), 1402–1415. https://doi.org/10.1016/j.envsoft.2005.07.004.
Kumar, S.V., Mocko, D.M., Wang, S., Peters-Lidard, C.D., Borak, J., 2019. Assimilation of remotely sensed Leaf Area Index into the Noah-MP land surface model: Impacts on water and carbon fluxes and states over the Continental U.S. J. Hydrometeorol. https://doi.org/10.1175/JHM-D-18-0237.1.
Kumar, S.V., Reichle, R.H., Peters-Lidard, C.D., Koster, R.D., Zhan, X., Crow, W.T., Eylander, J.B., Houser, P.R., 2008. A land surface data assimilation framework using the land information system: Description and applications. Adv. Water Resour. 31 (11), 1419–1432. https://doi.org/10.1016/j.advwatres.2008.01.013.
Kumar, S., Mocko, D., Vuyovich, C., Peters-Lidard, C., 2020. Impact of surface albedo assimilation on snow estimation. Remote Sens. 12 (4), 645. https://doi.org/10.3390/rs12040645.
Kumi-Boateng, B., Mireku-Gyimah, D., & Duker, A. A. (2012). A Spatio-Temporal Based Estimation of Vegetation Changes in the Tarkwa Mining Area of Ghana. 15.
Ling, X.L., Fu, C.B., Guo, W.D., Yang, Z.-L., 2019. Assimilation of remotely sensed LAI Into CLM4CN Using DART. J. Adv. Model. Earth Syst. https://doi.org/10.1029/2019MS001634.
Liston, G.E., Pielke, R.A., Greene, E.M., 1999. Improving first-order snow-related deficiencies in a regional climate model. J. Geophys. Res.: Atmosph. 104 (D16), 19559–19567. https://doi.org/10.1029/1999JD900055.
Littell, J.S., McKenzie, D., Kerns, B.K., Cushman, S., Shaw, C.G., 2011. Managing uncertainty in climate-driven ecological models to inform adaptation to climate change. Ecosphere 2 (9), art102. https://doi.org/10.1890/ES11-00114.1.
Maggioni, V., Houser, P.R., 2017. Soil Moisture Data Assimilation. In: Data Assimilation for Atmospheric, Oceanic and Hydrologic Applications Vol. III. Springer, pp. 195–217.
Maggioni, V., Reichle, R.H., Anagnostou, E.N., 2011. The effect of satellite rainfall error modeling on soil moisture prediction uncertainty. J. Hydrometeorol. 12 (3), 413–428. https://doi.org/10.1175/2011JHM1355.1.
Maggioni, V., Reichle, R.H., Anagnostou, E.N., 2012. The impact of rainfall error characterization on the estimation of soil moisture fields in a land data assimilation system. J. Hydrometeorol. 13 (3), 1107–1118. https://doi.org/10.1175/JHM-D-11-0115.1.
Maggioni, V., Reichle, R.H., Anagnostou, E.N., 2013. The efficiency of assimilating satellite soil moisture retrievals in a land data assimilation system using different rainfall error models. J. Hydrometeorol. 14 (1), 368–374. https://doi.org/10.1175/JHM-D-12-0105.1.
Masutani, M., Schlatter, T.W., Errico, R.M., Stoffelen, A., Andersson, E., Lahoz, W., Woollen, J.S., Emmitt, G.D., Riishøjgaard, L.-P., Lord, S.J., 2010. Observing System Simulation Experiments. In: Lahoz, W., Khattatov, B., Menard, R. (Eds.), Data Assimilation. Springer, Berlin Heidelberg, pp. 647–679. https://doi.org/10.1007/978-3-540-74703-1_24.
Mitchell, K.E., 2004. The multi-institution North American Land Data Assimilation System (NLDAS): Utilizing multiple GCIP products and partners in a continental distributed hydrological modeling system. J. Geophys. Res. 109 (D7). https://doi.org/10.1029/2003JD003823.
Niu, G.-Y., Yang, Z.-L., 2007. An observation-based formulation of snow cover fraction and its evaluation over large North American river basins. J. Geophys. Res. 112 (D21). https://doi.org/10.1029/2007JD008674.
Niu, G.-Y., Yang, Z.-L., Mitchell, K. E., Chen, F., Ek, M. B., Barlage, M., Kumar, A., Manning, K., Niyogi, D., Rosero, E., Tewari, M., & Xia, Y. (2011). The community Noah land surface model with multiparameterization options (Noah-MP): 1. Model description and evaluation with local-scale measurements. Journal of Geophysical Research, 116(D12). https://doi.org/10.1029/2010JD015139.
Peterson, D. W., Kerns, B. K., & Dodson, E. K. (2014). Climate change effects on vegetation in the Pacific Northwest: A review and synthesis of the scientific literature and simulation model projections.
Rajib, A., Kim, I.L., Golden, H.E., Lane, C.R., Kumar, S.V., Yu, Z., Jeyalakshmi, S., 2020. Watershed modeling with remotely sensed big data: MODIS leaf area index improves hydrology and water quality predictions. Remote Sens. 12 (13), 2148. https://doi.org/10.3390/rs12132148.
Rees, W.G., Danks, F.S., 2007. Derivation and assessment of vegetation maps for reindeer pasture analysis in Arctic European Russia. Polar Rec. 43 (04). https://doi.org/10.1017/S0032247407006420.
Reichle, R.H., 2008. Data assimilation methods in the Earth sciences. Adv. Water Resour. 31 (11), 1411–1418. https://doi.org/10.1016/j.advwatres.2008.01.001.
Reichle, R.H., Crow, W.T., Keppenne, C.L., 2008. An adaptive ensemble Kalman filter for soil moisture data assimilation: Adaptive ensemble filter for soil moisture assimilation. Water Resour. Res. 44 (3). https://doi.org/10.1029/2007WR006357.
Singh, V., Xiaosheng, Q., 2019. Data assimilation for constructing long-term gridded daily rainfall time series over Southeast Asia. Clim. Dyn. 53 (5–6), 3289–3313. https://doi.org/10.1007/s00382-019-04703-6.
Steinschneider, S., Ray, P., Rahat, S.H., Kucharski, J., 2019. A weather-regime-based stochastic weather generator for climate vulnerability assessments of water systems in the Western United States. Water Resour. Res. 55 (8), 6923–6945. https://doi.org/10.1029/2018WR024446.
Sun, C., 2004. A methodology for snow data assimilation in a land surface model. J. Geophys. Res. 109 (D8). https://doi.org/10.1029/2003JD003765.
Tucker, C.J., Pinzon, J.E., Brown, M.E., Slayback, D.A., Pak, E.W., Mahoney, R., Vermote, E.F., El Saleous, N., 2005. An extended AVHRR 8-km NDVI dataset compatible with MODIS and SPOT vegetation NDVI data. Int. J. Remote Sens. 26 (20), 4485–4498. https://doi.org/10.1080/01431160500168686.
Walker, J.P., Houser, P.R., Reichle, R.H., 2003. New technologies require advances in hydrologic data assimilation. Eos, Trans. Am. Geophys. Union 84 (49), 545. https://doi.org/10.1029/2003EO490002.
Weaver, C., da Silva, A., Chin, M., Ginoux, P., Dubovik, O., Flittner, D., Zia, A., Remer, L., Holben, B., Gregg, W., 2007. Direct insertion of MODIS radiances in a global aerosol transport model. J. Atmos. Sci. 64 (3), 808–827. https://doi.org/10.1175/JAS3838.1.
Wullschleger, S.D., Epstein, H.E., Box, E.O., Euskirchen, E.S., Goswami, S., Iversen, C.M., Kattge, J., Norby, R.J., van Bodegom, P.M., Xu, X., 2014. Plant functional types in Earth system models: Past experiences and future directions for application of dynamic vegetation models in high-latitude ecosystems. Ann. Bot. 114 (1), 1–16. https://doi.org/10.1093/aob/mcu077.
Xia, Y., Mitchell, K., Ek, M., Sheffield, J., Cosgrove, B., Wood, E., Luo, L., Alonge, C., Wei, H., Meng, J., Livneh, B., Lettenmaier, D., Koren, V., Duan, Q., Mo, K., Fan, Y., & Mocko, D. (2012). Continental-scale water and energy flux analysis and validation for the North American Land Data Assimilation System project phase 2 (NLDAS-2): 1. Intercomparison and application of model products: WATER AND ENERGY FLUX ANALYSIS. Journal of Geophysical Research: Atmospheres, 117(D3), n/a-n/a. https://doi.org/10.1029/2011JD016048.
Xiao, Z., Liang, S., Wang, J., Xiang, Y., Zhao, X., Song, J., et al., 2016. Long-Time-Series Global Land Surface Satellite Leaf Area Index Product Derived From MODIS and AVHRR Surface Reflectance. IEEE Trans. Geosci. Remote Sens. 54 (9), 5301–5318. https://doi.org/10.1109/TGRS.2016.2560522.
Xue, Y., Houser, P.R., Maggioni, V., Mei, Y., Kumar, S.V., Yoon, Y., 2019. Assimilation of satellite-based snow cover and freeze/thaw observations over high mountain Asia. Front. Earth Sci. 7. https://doi.org/10.3389/feart.2019.00115.
Yang, M.-S., Wu, M.-C., & Liu, J.-K. (2012). Analysis of spatial characteristics for landslides vegetation restoration monitoring by LiDAR surface roughness data and multispectrum imagery. 7561–7564. https://doi.org/10.1109/IGARSS.2012.6351912.
Yoon, Y., Kumar, S.V., Forman, B.A., Zaitchik, B.F., Kwon, Y., Qian, Y., Rupper, S., Maggioni, V., Houser, P., Kirschbaum, D., Richey, A., Arendt, A., Mocko, D., Jacob, J., Bhanja, S., Mukherjee, A., 2019. Evaluating the uncertainty of terrestrial water budget components over high Mountain Asia. Front. Earth Sci. 7. https://doi.org/10.3389/feart.2019.00120.
Zhang, X., Maggioni, V., Rahman, A., Houser, P., Xue, Y., Sauer, T., Kumar, S., Mocko, D., 2020. The influence of assimilating leaf area index in a land surface model on global water fluxes and storages. Hydrol. Earth Syst. Sci. 24 (7), 3775–3788. https://doi.org/10.5194/hess-24-3775-2020.